RSC Advances

PAPER

View Article Online
View Journal | View Issue

Open Access Article. Published on 27 March 2017. Downloaded on 12/4/2025 9:40:58 PM.
This article is licensed under a Creative Commons Attribution 3.0 Unported Licence.

Check for updates

Cite this: *RSC Adv.*, 2017, **7**, 18270

In situ formation of pH-responsive Prussian blue for photoacoustic imaging and photothermal therapy of cancer†

Ming Cheng,‡[a] Wei Peng,‡[a] Peng Hua,[a] Zhengrong Chen,*[a] Jia Sheng,[a] Juan Yang *[b] and Yongyou Wu*[a]

Received 15th February 2017
Accepted 9th March 2017

DOI: 10.1039/c7ra01879g

rsc.li/rsc-advances

Designing theranostic agents that are responsive to weakly acidic tumor microenvironments for optimized imaging and therapeutic effects is of great interest in nanomedicine. In the current study, we constructed a pH-triggered smart theranostic system based on pH-responsive Prussian blue, which shows good performance in the photoacoustic imaging (PAI)-guided photothermal therapy (PTT) of tumors. Precursors to Prussian blue, namely ferrous and ferricyanide ions, were separately encapsulated into pH-responsive hydrogels that only degraded under acidic conditions. *In vitro* results showed that the encapsulated ions were gradually released in acidic buffer, accompanied by hydrogel degradation. After the resultant hydrogel was mixed and intratumorally injected into tumor-bearing mice, the encapsulated ferrous ions and ferricyanide ions were successfully released in the acidic tumor environment, allowing the *in situ* formation of Prussian blue in the tumor area. This provided an efficient theranostic agent for PAI-guided PTT of cancer. Our research highlights the potential of Prussian blue-based theranostic agents for the precise diagnosis and treatment of cancer.

Introduction

Nanotheranostic agents integrated with different therapeutic and diagnostic functions have attracted considerable interest due to their great potential in the field of precision cancer medicine.[1–4] Many theranostic agents have been developed for simultaneous use in different imaging and therapeutic technologies, including magnetic resonance imaging-photothermal therapy (MRI-PTT),[5–10] optical imaging-photodynamic therapy (OI-PDT),[11,12] MRI-chemotherapy,[13] computed tomography (CT)-PTT,[14–16] and photoacoustic imaging (PAI)–PTT.[10,17–19] However, most of these theranostic agents are fabricated by the combination of individual functional agents due to the different principles of imaging and therapy technologies. The major problem with these theranostic agents is that the individual functional agents can detach from each other *in vivo*, leading to inaccurate diagnosis and poor efficacy. Therefore, the development of theranostic agents based on single materials that can serve as both imaging and therapeutic agents is important.

Near-infrared (NIR) absorbing materials are materials that have strong absorption in the NIR region. Due to the deep tissue penetration of NIR light, NIR absorbing materials have been widely investigated for *in vivo* applications,[2,20–22] particularly photothermal therapy, which employs NIR materials to absorb NIR light and generate heat, leading to thermal ablation of malignant cells. Coincidentally, NIR adsorption-induced heat can also lead to transient thermoelastic expansion, generating ultrasonic waves detectable by ultrasonic detectors. Therefore, NIR-absorbing materials are good candidates for photoacoustic imaging (PAI) contrast agents. Consequently, the combination of PTT and PAI provides a potential solution to the aforementioned problem with theranostic agents, as both the imaging technology and therapeutic method are based on the same NIR-absorbing material. Moreover, as a promising alternative to traditional cancer therapies, PTT has received significant attention in recent years due to its high selectivity toward targeting sites and noninvasiveness in normal tissues. PAI has many advantages in comparison with traditional optical imaging methods, including low signal scattering in tissues, high resolution, and sensitivity. Therefore, the combination of PTT and PAI shows great promise for optimizing diagnostic accuracy and therapeutic efficiency.

In the last decade, many NIR-absorbing nanomaterials, including gold nanostructures,[23–26] carbon-based nanomaterials,[27–32] transition-metal oxides and sulfides,[15,33–37] upconversion nanoparticles,[38,39] and various organic polymers,[40–44] have shown promise as PTT and PAI agents, both *in vitro* and *in vivo*.

[a]*Department of General Surgery, The Second Affiliated Hospital of Soochow University, Suzhou 215007, China. E-mail: chen_zr@126.com; wuyoyo@aliyun.com*

[b]*Sanitation & Environment Technology Institute, Soochow University, Suzhou 215123, China. E-mail: yang_juan8726@163.com*

† Electronic supplementary information (ESI) available: Detailed experimental procedures and supplementary data. See DOI: 10.1039/c7ra01879g

‡ These two authors contributed equally to this work.

This journal is © The Royal Society of Chemistry 2017

Open Access Article. Published on 27 March 2017. Downloaded on 12/4/2025 9:40:58 PM.
This article is licensed under a Creative Commons Attribution 3.0 Unported Licence.

However, due to the stable physicochemical properties under physiological/tumor conditions, most of these nanotheranostic agents have the same effect when accumulated in tumor and normal tissue, leading to low specificity in both tumor imaging and tumor therapy. Ideal nanotheranostic agents would only be functional in the desired tumor area. In comparison to inert theranostic agents, microenvironment-sensitive materials, such as pH- or enzyme-responsive materials, have many advantages in both imaging and therapy. For instance, in optical imaging, pH-responsive fluorescence probes can increase the signal-to-noise ratio in the region of interest, which increases detection sensitivity and diagnosis accuracy.[45–47] Furthermore, in cancer chemotherapy, tumor microenvironment-responsive drugs not only enhance the therapeutic effect, but also decrease the side effects on normal tissues.[48,49] In a previous investigation, we developed pH-responsive Fe–gallic-acid nanoparticles for the PAI-guided PTT of cancer.[17] Due to their pH-sensitive properties, Fe–gallic acid nanoparticles have long retention times in tumors with mild acidic conditions and can easily be decomposed and metabolized in normal organs, such as the liver and spleen. This makes them a safe and promising candidate for a PAI–PTT theranostic agent. The above studies clearly demonstrate the remarkable advantages of microenvironment-sensitive theranostic agents when extended to clinical applications.

Following our previous study, we now report a novel *in situ*-formed pH-responsive PAI–PTT theranostic agent based on Prussian blue complex, which possesses strong NIR absorbance under acidic conditions. As shown in Fig. 1, ferrous ions and ferricyanide ions were separately encapsulated in an injectable pH-responsive hydrogel based on the Schiff base reaction of dibenzaldehyde-terminated telechelic poly(ethylene glycol) (DF-PEG) and glycol chitosan.[50] After being mixed and injected into the tumor, the resultant hydrogels can be degraded under weakly acidic conditions and release ferrous ions and ferricyanide ions to form Prussian blue *in situ*, leading to excellent *in vivo* photoacoustic imaging and a good photothermal therapy effect against tumors in mice. To our knowledge, such an *in situ*-formed pH-responsive theranostic agent for imaging guided therapy applications has not been reported previously.

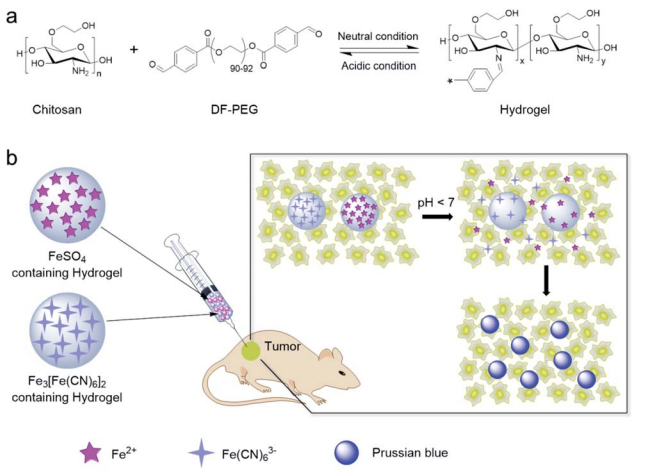

Fig. 1 Schematic illustration of (a) formation of pH-responsive hydrogel, and (b) *in situ* formation of Prussian blue in the tumor area.

Experimental

Chemicals

Glycol chitosan was purchased from Sigma-Aldrich. Ferrous sulfate and potassium ferricyanide were purchased from Aladdin Industrial Corporation. Dibenzaldehyde-terminated poly(ethylene glycol) (DF-PEG) was provided by Dr. Yangyun Wang. Other analytical grade chemicals were purchased from Sinopharm Chemical Reagent Co., Ltd and used as received.

Synthesis of Prussian blue complex

Prussian blue complex was prepared by mixing $FeSO_4$ and $K_3[Fe(CN)_6]$ solutions. In a typical synthesis, $FeSO_4$ (3 mL, 10 mM) was mixed with deionized water (45 mL) before adding $K_3[Fe(CN)_6]$ (2 mL, 10 mM) and mixing until homogeneous to obtain Prussian blue complex.

Hydrogel preparation

Glycol chitosan (30 mg mL^{-1}) and DF-PEG solution (200 mg mL^{-1}) were prepared separately by dissolving certain amounts, respectively, in 4-(2-hydroxyethyl)-1-piperazineethanesulfonic acid (HEPES) buffer (pH 7.0). To obtain the ferrous-ion-containing hydrogel, glycol chitosan (100 μL), deionized water (100 μL), $FeSO_4$ (300 μL, 10 mM), and DF-PEG (100 μL) were mixed in a 1 mL syringe. The precursor solutions in the syringe were kept at room temperature for 3 h to allow gelation. The ferricyanide containing hydrogel was prepared similarly, by mixing glycol chitosan (100 μL), deionized water (200 μL), $K_3[Fe(CN)_6]$ (200 μL, 10 mM), and DF-PEG (100 μL), according to the above procedure. After the hydrogels were formed, hydrogel fragments were obtained under extrusion by slowly evacuating the syringe.

In vitro photothermal performance

Prussian blue solutions (1 mL) of different concentrations were irradiated using an 808 nm laser with a power density of 0.5 W cm^{-2}. The solution temperature was measured with an infrared camera (FLIR A65) at 100 ms intervals for a total of 10 min.

In vitro photoacoustic effect

The photoacoustic performance of Prussian blue was determined using a commercial multispectral optoacoustic tomography system (MSOT, iThera Medical, inVision 256). This system was equipped with an array of 256 cylindrically focused transducers to detect photoacoustic signals. A tunable laser system (680–980 nm, 10 Hz repetition rate, 8 ns pulse width, 120 mJ pulse peak energy) was used to excite the target object with optical pulses to generate the photoacoustic effect. *In vitro* photoacoustic imaging of Prussian blue at different concentrations was performed using an excitation wavelength of 720 nm. Photoacoustic signal intensities were measured by region of interest (ROI) analysis using the MSOT imaging system software package.

Open Access Article. Published on 27 March 2017. Downloaded on 12/4/2025 9:40:58 PM.
This article is licensed under a Creative Commons Attribution 3.0 Unported Licence.

In vitro pH-responsive properties of Prussian blue and hydrogels

To evaluate the pH-responsive properties of Prussian blue complex, $FeSO_4$ (1 mM) and $K_3[Fe(CN)_6]$ (1 mM) were directly mixed in deionized water in a 3 : 2 molar ratio to form Prussian blue. The as-prepared complex was then added to different buffers (pH 7.2, 6.8, 6.4, 6.1, 5.6, and 5.0) to give final Prussian blue concentrations of 100 μM. The absorbances of the resultant Prussian blue solutions were determined at different time points after mixing. To demonstrate the pH-responsive ability of the hydrogel, ferrous ions containing hydrogel fragments (50 μL) and ferricyanide containing hydrogel fragments (50 μL) were mixed in different buffers (1.8 mL; pH 7.2, 6.1, 5.6, and 5.0). The absorbances and photoacoustic signals of each sample were monitored at different time points.

Biocompatibility evaluation

4T1 murine breast cancer cells were used to investigate the cytotoxicity of Prussian blue, glycol chitosan, and DF-PEG using the standard MTT assay. To evaluate the biocompatibility of the formed hydrogel, glycol chitosan (100 μL) and DF-PEG (100 μL) were first mixed with HEPES buffer (400 μL, pH 7.0) and then immediately transferred into six-well plates. After gelation for 3 h at room temperature, 1×10^5 4T1 cells were seeded into the hydrogel membrane, covered, and incubated with standard cell media at 37 °C in a 5% CO_2 atmosphere. The adherence of 4T1 cells on the hydrogel membrane was observed by an optical microscope and compared with cells cultured in normal six-well plates.

Animal model

The tumor models used were established by subcutaneous injection of 4T1 cell suspension (50 μL, ~5×10^6 cells) into the right back of male Balb/c mice. By monitoring tumor growth, mice bearing ~100 mm^3 tumors were selected for imaging and therapy experiments. All animal experiments were performed in accordance with the ethical guidelines of Soochow University and protocols approved by the Soochow University Laboratory Animal Center.

Photoacoustic (PA) imaging

Prior to *in vivo* PA imaging, the tumor-bearing mice were anesthetized with isoflurane. After intratumoral injection with 50 μL of 1 : 1 mixed hydrogel fragments (volume ratio of ferrous ions and ferricyanide containing hydrogel fragments), the mice were transferred into a 34 °C water bath to maintain their body temperature. An excitation wavelength of 720 nm was adopted to acquire PA images at different time points post-injection. Ten frames were obtained for each position and averaged to minimize the influence of animal movement in the images.

Photothermal therapy

Twenty tumor-bearing Balb/c mice with an average tumor volume of ~100 mm^3 were randomly allocated into four groups. Mice in the treatment group underwent intratumoral injection with 50 μL of 1 : 1 mixed hydrogel fragments. For the control groups, mice were treated with the same volume of saline. Laser-treated groups were irradiated with an 808 nm NIR laser (Hi-Tech Optoelectronics Co., Ltd. Beijing, China) with a power density of 1 W cm^{-2} for 10 min. During irradiation, real-time thermal images of the tumor area were acquired using an infrared camera (FLIR A65). Tumor sizes were measured daily and calculated as the volume equal to $a \times b^2/2$, where a and b represent the length and width of the tumor, respectively. Relative tumor volumes were obtained by dividing with the initial tumor size before laser treatment.

Results and discussion

Prussian blue is an ancient low-cost dye with a simple preparation. Due to the strong optical absorbance in the near-infrared region (NIR), Prussian blue-based nanoparticles have been developed as potential photothermal agents for PTT of cancers.[6,7] Typically, Prussian blue is easily obtained by directly mixing ferric ion and ferrocyanide ion solution. Because ferric ions are easily hydrolyzed, Prussian blue formation can be difficult under neutral or weakly acidic conditions. Therefore, to ensure that the formation of Prussian blue was feasible under physiological conditions, ferrous ions and ferricyanide ions were adopted as precursors for the synthesis of Prussian blue in the current study, because the hydrolysis pH of ferrous ions (7.5) is much higher than that of ferric ions (2.9). Fig. 2a shows UV-Vis-NIR spectra of Prussian blue obtained by mixing $FeSO_4$ and $K_3[Fe(CN)_6]$ solutions stoichiometrically, which exhibited a blue color and a wide absorption band that extended from 500–1000 nm and peaked at 720 nm. Due to its strong NIR absorption, Prussian blue has obvious photothermal and photoacoustic effects. As shown in Fig. 2b and S1,† the temperature of aqueous solutions containing different concentrations of

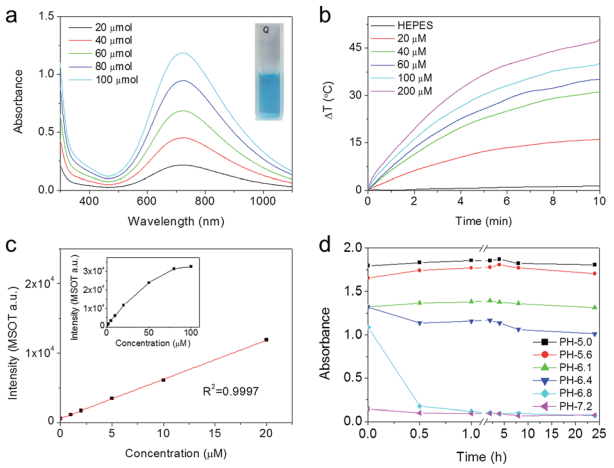

Fig. 2 (a) UV-Vis-NIR absorbance spectra of Prussian blue solutions with different concentrations. Inset: photographs of Prussian blue solutions. (b) Temperature elevation of different Prussian blue concentrations as a function of irradiation time. (c) Photoacoustic signals of Prussian blue at 720 nm as a function of concentration. (d) Absorbance variation of Prussian blue at 720 nm in different pH buffer solutions.

Open Access Article. Published on 27 March 2017. Downloaded on 12/4/2025 9:40:58 PM.
This article is licensed under a Creative Commons Attribution 3.0 Unported Licence.

Prussian blue could be rapidly increased by irradiation with an 808 nm laser (0.5 W m^{-2}), in remarkable contrast to the temperature of pure water under the same irradiation conditions. The results shown in Fig. S2† further demonstrate that ΔT can be controlled by simply tuning the Prussian blue concentration from 20 to 200 μM. After irradiation for 10 min, the temperature of the Prussian blue solution at a concentration of 200 μM increased by 46 °C. Photoacoustic enhancements of performance in a series of Prussian blue solutions with different concentrations are shown in Fig. 2c and S3.† The photoacoustic signal increased with increasing concentration from 0 to 100 μM, indicating that Prussian blue would be a good candidate for photoacoustic imaging. Furthermore, NIR absorption exhibited a strong pH dependency, as shown in Fig. 2d and S4.† In general, the absorbance gradually decreased as the pH increased from 5.0 to 7.0. The remarkable dependency of NIR absorption on pH was well suited to the weakly acidic microenvironment of tumors, giving Prussian blue the potential to be a smart theranostic agent for tumors through PAI-guided PTT.

To construct the pH-triggered smart theranostic agent, the precursors of Prussian blue, ferrous and ferricyanide ions, were separately encapsulated into pH-responsive hydrogels based on the Schiff base reaction of dibenzaldehyde-terminated telechelic poly(ethylene glycol) (PEG) and glycol chitosan. As the formed acylhydrazone bond was easily hydrolyzed under weakly acidic conditions, the hydrogel gradually degraded in acidic buffer solution, as shown in Fig. S5.† Therefore, by mixing the ferrous and ferricyanide ion-containing hydrogels in acidic buffer, the encapsulated ions were gradually released to form Prussian blue, accompanied by degradation of the hydrogels. Fig. 3a shows photographs of the mixed hydrogels after incubation in buffers with different pH values for different time periods. The mixture colors showed a strong pH-dependent effect, exhibiting an obvious blue color when the pH was lower than 6.1, indicating Prussian blue formation in acidic buffer. Quantified UV-Vis-NIR measurements are shown in Fig. 3b, S6, and S7.† The absorbance at 720 nm of the mixed hydrogel in pH 7.0 buffer showed no appreciable change as incubation time increased, while the absorbance markedly increased with decreasing pH. Furthermore, the results also indicated fast hydrogel degradation and the release of encapsulated ions as the absorbance increased rapidly, reaching a plateau within 4 h of incubation. After being incubated in pH 5.0 buffer for 24 h, more than 90% of the encapsulated ions were released according to the calculation. Due to the strong pH-dependent absorption of the mixed hydrogel, photoacoustic imaging of mixed hydrogel dispersed in buffer solutions with different pH values was carried out (Fig. 3c and d). PAI was captured at 720 nm, which corresponded with the absorption peak of Prussian blue. The photoacoustic signal showed an obvious increase as the pH value decreased, which was consistent with the variation in absorbance. The above results suggested that the constructed probe could potentially serve as a pH-triggered smart theranostic agent for cancer.

In addition to outstanding physicochemical properties, biocompatibility was essential for the *in vivo* application of the resultant theranostic agents. To evaluate their biocompatibility,

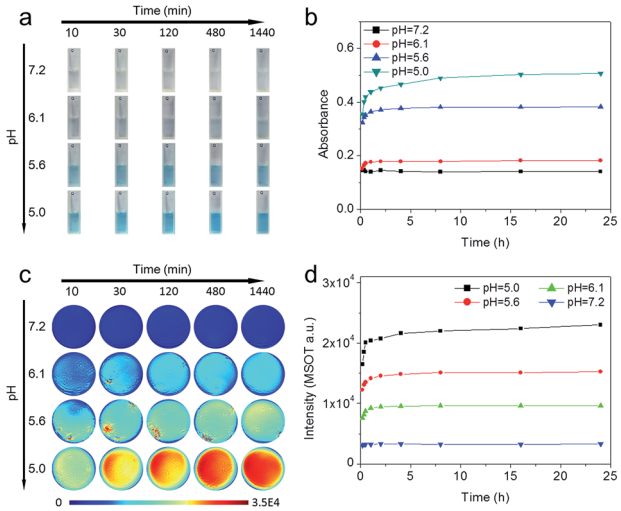

Fig. 3 (a) Photographs of mixed ferrous ion-containing hydrogel and ferricyanide ion-containing hydrogel after incubation in buffers with different pH values for different time periods. (b) Absorbance at 720 nm of hydrogel mixture incubated in different pH buffer, as shown in (a). (c) Photoacoustic imaging of hydrogel mixtures after incubation in buffers with different pH values for different time periods. (d) Quantified photoacoustic signals of hydrogel mixtures incubated in different pH buffers, as shown in (c).

4T1 cells (murine breast cancer cells) were adopted to investigate the potential cytotoxicity of the precursors for theranostic agents through a standard tetrazolium-based colorimetric assay (MTT). As shown in Fig. 4a–c, the concentrations required for 80% cell viability were 5 mg mL^{-1}, 0.5 mg mL^{-1}, and 100 μM for glycol chitosan, DF-PEG, and Prussian blue, respectively, indicating that the precursors were nontoxic to cells at the investigated concentrations. Furthermore, the 4T1 cells adhered well after being seeded into the hydrogel-membrane-covered six-well

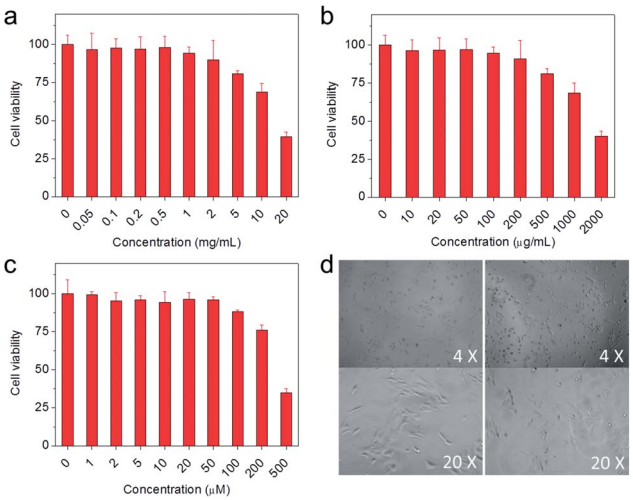

Fig. 4 (a–c) Relative cell viabilities of 4T1 cells after incubation with various concentrations of glycol chitosan, DF-PEG, and Prussian blue, respectively. (d) Bright field photographs of 4T1 cells after being cultured in normal plates (left panel) and hydrogel membrane-covered plates (right panel).

Open Access Article. Published on 27 March 2017. Downloaded on 12/4/2025 9:40:58 PM.
This article is licensed under a Creative Commons Attribution 3.0 Unported Licence.

plates (right panel of Fig. 4d), which showed no obvious differences compared with the cells cultured in normal plates without hydrogel (left panel of Fig. 4d), indicating that the hydrogel had a negligible effect on 4T1 cell viability. These results showed that all components of the theranostic agent were nontoxic, suggesting the resultant theranostic agent had great potential for *in vivo* applications.

Encouraged by the pH-dependent photoacoustic signals and good biocompatibility, we carried out further *in vivo* photoacoustic imaging on a subcutaneous 4T1 tumor model *via* intratumoral injection of the hydrogel mixture (ferrous ion-containing hydrogel and ferricyanide ion-containing hydrogel). Photoacoustic images acquired at different time points post-injection are shown in Fig. 5a. Compared with the image obtained pre-injection, the overall contrast of the tumor area was gradually enhanced, showing a maximum signal at around 4 h post-injection, indicating the gradual release of ferrous ions and ferricyanide ions, and formation of Prussian blue, in the acidic tumor environment. Thereafter, the signal of the tumor area started to decrease, suggesting the *in situ* formed Prussian blue was gradually metabolized. To further quantitatively evaluate the imaging performance, the photoacoustic signals in the region of interest (ROI) of each image were calculated and presented in Fig. 5b. The variation tendency of photoacoustic signals in the tumor area was consistent with the *in vitro* photoacoustic results shown in Fig. 3d, further demonstrating the effectiveness of the current theranostic agent.

As mentioned previously, the PAI contrast agents could also serve as PTT agents for tumor therapy. Therefore, we further evaluated the photothermal effect of the constructed theranostic agent *in vivo*. According to the *in vivo* PAI results, mice bearing 4T1 tumors were anesthetized after intratumoral injection of hydrogel mixture for 4 h, the optimal time for Prussian blue formation in the tumor, and then exposed to 808 nm laser irradiation with a power density of 1.0 W cm^{-2}. An infrared imaging camera was used to monitor temperature changes at the tumor site under NIR irradiation. Under irradiation, the temperature of the tumor area increased by 16 °C within 10 min (Fig. 5c and d). In comparison, the tumor temperature of the control group (from the intratumoral injection of saline and irradiation under the same conditions) only increased by 3 °C, which was much less than the tumor injected with hydrogel mixture. For further comparison, the same amount of hydrogel mixture was also injected into subcutaneous muscle. Interestingly, the muscle temperature was markedly lower than that of the tumor after injection using the same hydrogel mixture dose and laser irradiation conditions. These results not only demonstrated the feasibility of tumor-pH-triggered theranostic agents for PAI-guided PTT therapy, but also indicated the potential of the constructed theranostic agent for reducing non-specific photothermal heating of normal tissues exposed to laser irradiation.

To fully assess the *in vivo* therapeutic potential of the Prussian blue-based theranostic agent, the photothermal therapeutic efficacy was further investigated. Balb/c mice with subcutaneous 4T1 tumors were selected as the animal model and randomly divided into four groups ($n = 5$). The treatment group underwent intratumoral injection with hydrogel mixture and was then irradiated with an 808 nm laser for 10 min with a power density of 1 W cm^{-2} at 4 h post-injection. The other three groups were the saline injection group, mice injected with saline and exposed to laser irradiation, and mice injected with hydrogel mixture without laser irradiation. For the treatment group, the tumor had shrunk markedly after one day of photothermal treatment, forming black scars that were completely eradicated after two weeks of treatment (Fig. 6a). In contrast, the tumors of the other three control groups grew with feeding

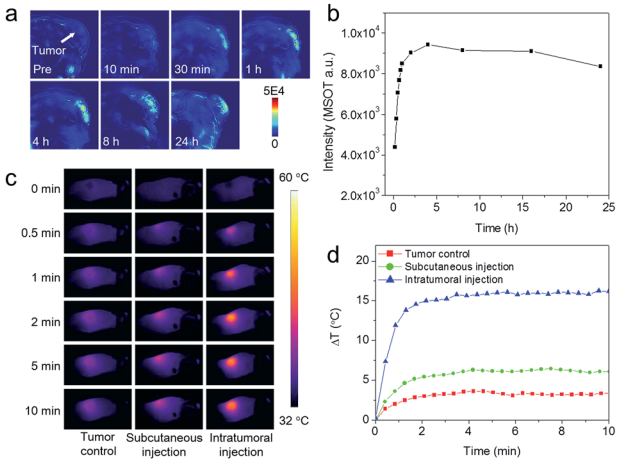

Fig. 5 (a) Photoacoustic images of tumor before injection and different time points post-injection of the hydrogel mixture. (b) Photoacoustic signal variations of the tumor site in (a) as a function of time post-injection. (c) Thermal images of mice after intratumoral injection of saline (column 1), subcutaneous injection of hydrogel mixture (column 2), or intratumoral injection of hydrogel mixture (column 3) after exposure to 808 nm laser irradiation (1.0 W cm^{-2}) for different time periods. (d) Temperature changes in the region of interest in mice during laser irradiation, as indicated in (c).

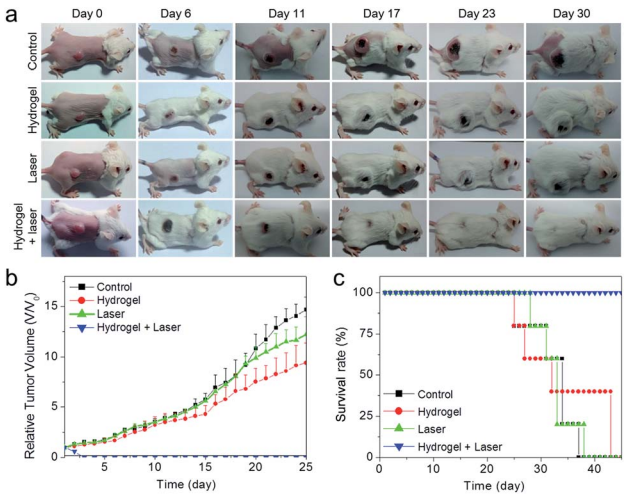

Fig. 6 (a) Representative photographs of mice bearing 4T1 tumors after the various treatments indicated. (b) Corresponding growth curves of 4T1 tumors in different groups of mice after treatment. The relative tumor volumes were normalized to their initial size. (c) Survival curves of mice after the various treatments indicated.

 This journal is © The Royal Society of Chemistry 2017

Open Access Article. Published on 27 March 2017. Downloaded on 12/4/2025 9:40:58 PM.
This article is licensed under a Creative Commons Attribution 3.0 Unported Licence.

time (Fig. 6b). Furthermore, the mice in the control groups had a mean lifespan of 33–35 days. This was shorter than that of the treated mice, which were tumor-free after treatment and deliberately sacrificed after 45 days (Fig. 6c). The above results suggested that *in situ* formed pH-responsive Prussian blue could serve as a powerful agent for *in vivo* photothermal cancer therapy.

Conclusions

In summary, a novel Prussian blue-based pH-responsive theranostic agent was successfully fabricated for PAI-guided PTT cancer therapy. In the system, the precursors of Prussian blue, namely ferrous ions and ferricyanide ions, were separately encapsulated into pH-responsive hydrogels. By mixing the resultant hydrogels under the acidic conditions, the encapsulated ions were rapidly released to form Prussian blue. Prussian blue exhibited strong pH-dependent NIR absorbance in the pH range 5.0–7.0, which was in perfect alignment with the weakly acidic microenvironment of tumors. After intratumoral injection into a mouse tumor model, the hydrogel was successfully degraded in the tumor environment, releasing ferrous and ferricyanide ions to form Prussian blue *in situ*, providing an efficient theranostic agent for PAI-guided PTT tumor therapy. Benefitting from the dual pH-responsive properties attributed to the hydrogels and Prussian blue, the current theranostic agent shows obvious advantages in reducing background signals in PAI imaging and non-specific photothermal heating of normal tissues in PTT therapy. Furthermore, all components in the current system have low toxicity, demonstrating the excellent biocompatibility of the resultant theranostic agent. Therefore, the current study provides a new strategy for constructing smart theranostic agents for cancer diagnosis and treatment through PAI–PTT.

Acknowledgements

This work was supported by the Youth Fund of the Project in Science and Education of Suzhou (kjxw2015009) and the National Natural Science Foundation of China (21406241). The authors wish to thank Dr Yangyun Wang from Sochoow University for providing the PEG derivatives.

References

1 G. Chen, I. Roy, C. Yang and P. N. Prasad, *Chem. Rev.*, 2016, **116**, 2826–2885.
2 Y. Chen, C. Tan, H. Zhang and L. Wang, *Chem. Soc. Rev.*, 2015, **44**, 2681–2701.
3 E. Terreno, F. Uggeri and S. Aime, *J. Controlled Release*, 2012, **161**, 328–337.
4 K. Yang, L. Z. Feng, X. Z. Shi and Z. Liu, *Chem. Soc. Rev.*, 2013, **42**, 530–547.
5 K. Yang, G. Yang, L. Chen, L. Cheng, L. Wang, C. Ge and Z. Liu, *Biomaterials*, 2015, **38**, 1–9.
6 G. Fu, W. Liu, Y. Li, Y. Jin, L. Jiang, X. Liang, S. Feng and Z. Dai, *Bioconjugate Chem.*, 2014, **25**, 1655–1663.
7 L. Cheng, H. Gong, W. Zhu, J. Liu, X. Wang, G. Liu and Z. Liu, *Biomaterials*, 2014, **35**, 9844–9852.
8 F. Y. Liu, X. X. He, H. D. Chen, J. P. Zhang, H. M. Zhang and Z. X. Wang, *Nat. Commun.*, 2015, **6**, 8003.
9 Z. Zhou, Y. Sun, J. Shen, J. Wei, C. Yu, B. Kong, W. Liu, H. Yang, S. Yang and W. Wang, *Biomaterials*, 2014, **35**, 7470–7478.
10 J. Yu, C. Yang, J. Li, Y. Ding, L. Zhang, M. Z. Yousaf, J. Lin, R. Pang, L. Wei, L. Xu, F. Sheng, C. Li, G. Li, L. Zhao and Y. Hou, *Adv. Mater.*, 2014, **26**, 4114–4120.
11 C. Yue, P. Liu, M. Zheng, P. Zhao, Y. Wang, Y. Ma and L. Cai, *Biomaterials*, 2013, **34**, 6853–6861.
12 K. Yang, H. Xu, L. Cheng, C. Sun, J. Wang and Z. Liu, *Adv. Mater.*, 2012, **24**, 5586–5592.
13 Y. Chen, K. Ai, J. Liu, G. Sun, Q. Yin and L. Lu, *Biomaterials*, 2015, **60**, 111–120.
14 L. Cheng, J. Liu, X. Gu, H. Gong, X. Shi, T. Liu, C. Wang, X. Wang, G. Liu, H. Xing, W. Bu, B. Sun and Z. Liu, *Adv. Mater.*, 2014, **26**, 1886–1893.
15 G. Tian, X. Zhang, X. Zheng, W. Yin, L. Ruan, X. Liu, L. Zhou, L. Yan, S. Li, Z. Gu and Y. Zhao, *Small*, 2014, **10**, 4160–4170.
16 Z. Zhou, B. Kong, C. Yu, X. Shi, M. Wang, W. Liu, Y. Sun, Y. Zhang, H. Yang and S. Yang, *Sci. Rep.*, 2014, **4**, 3653.
17 J. Zeng, M. Cheng, Y. Wang, L. Wen, L. Chen, Z. Li, Y. Wu, M. Gao and Z. Chai, *Adv. Healthcare Mater.*, 2016, **5**, 772–780.
18 P. Huang, J. Lin, W. Li, P. Rong, Z. Wang, S. Wang, X. Wang, X. Sun, M. Aronova, G. Niu, R. D. Leapman, Z. Nie and X. Chen, *Angew. Chem., Int. Ed.*, 2013, **52**, 13958–13964.
19 D. Chen, C. Wang, X. Nie, S. Li, R. Li, M. Guan, Z. Liu, C. Chen, C. Wang, C. Shu and L. Wan, *Adv. Funct. Mater.*, 2014, **24**, 6621–6628.
20 D. Jaque, L. Martinez Maestro, B. del Rosal, P. Haro-Gonzalez, A. Benayas, J. L. Plaza, E. Martin Rodriguez and J. Garcia Sole, *Nanoscale*, 2014, **6**, 9494–9530.
21 A. Yuan, J. H. Wu, X. L. Tang, L. L. Zhao, F. Xu and Y. Q. Hu, *J. Pharm. Sci.*, 2013, **102**, 6–28.
22 L. Y. Rizzo, B. Theek, G. Storm, F. Kiessling and T. Lammers, *Curr. Opin. Biotechnol.*, 2013, **24**, 1159–1166.
23 B. Jang, J.-Y. Park, C.-H. Tung, I.-H. Kim and Y. Choi, *ACS Nano*, 2011, **5**, 1086–1094.
24 S. Wang, P. Huang, L. Nie, R. Xing, D. Liu, Z. Wang, J. Lin, S. Chen, G. Niu, G. Lu and X. Chen, *Adv. Mater.*, 2013, **25**, 3055–3061.
25 H. Li, X. Liu, N. Huang, K. Ren, Q. Jin and J. Ji, *ACS Appl. Mater. Interfaces*, 2014, **6**, 18930–18937.
26 J. Shen, H.-C. Kim, C. Mu, E. Gentile, J. Mai, J. Wolfram, L.-n. Ji, M. Ferrari, Z.-w. Mao and H. Shen, *Adv. Healthcare Mater.*, 2014, **3**, 1629–1637.
27 K. Yang, S. Zhang, G. Zhang, X. Sun, S.-T. Lee and Z. Liu, *Nano Lett.*, 2010, **10**, 3318–3323.
28 Y. Wang, K. Wang, J. Zhao, X. Liu, J. Bu, X. Yan and R. Huang, *J. Am. Chem. Soc.*, 2013, **135**, 4799–4804.
29 G. Gollavelli and Y.-C. Ling, *Biomaterials*, 2014, **35**, 4499–4507.
30 S. Wang, Q. Zhang, X. F. Luo, J. Li, H. He, F. Yang, Y. Di, C. Jin, X. G. Jiang, S. Shen and D. L. Fu, *Biomaterials*, 2014, **35**, 9473–9483.

Open Access Article. Published on 27 March 2017. Downloaded on 12/4/2025 9:40:58 PM.
This article is licensed under a Creative Commons Attribution 3.0 Unported Licence.

31 J. T. Robinson, K. Welsher, S. M. Tabakman, S. P. Sherlock, H. Wang, R. Luong and H. Dai, *Nano Res.*, 2010, **3**, 779–793.
32 C. Liang, S. Diao, C. Wang, H. Gong, T. Liu, G. Hong, X. Shi, H. Dai and Z. Liu, *Adv. Mater.*, 2014, **26**, 5646–5652.
33 L. Wen, L. Chen, S. Zheng, J. Zeng, G. Duan, Y. Wang, G. Wang, Z. Chai, Z. Li and M. Gao, *Adv. Mater.*, 2016, **28**, 5072–5079.
34 Y. Wang, Y. Wu, Y. Liu, J. Shen, L. Lv, L. Li, L. Yang, J. Zeng, Y. Wang, L. W. Zhang, Z. Li, M. Gao and Z. Chai, *Adv. Funct. Mater.*, 2016, **26**, 5335–5344.
35 X. Ding, C. H. Liow, M. Zhang, R. Huang, C. Li, H. Shen, M. Liu, Y. Zou, N. Gao, Z. Zhang, Y. Li, Q. Wang, S. Li and J. Jiang, *J. Am. Chem. Soc.*, 2014, **136**, 15684–15693.
36 J. Liu, X. P. Zheng, L. Yan, L. J. Zhou, G. Tian, W. Y. Yin, L. M. Wang, Y. Liu, Z. B. Hu, Z. J. Gu, C. Y. Chen and Y. L. Zhao, *ACS Nano*, 2015, **9**, 696–707.
37 W. Yin, L. Yan, J. Yu, G. Tian, L. Zhou, X. Zheng, X. Zhang, Y. Yong, J. Li, Z. Gu and Y. Zhao, *ACS Nano*, 2014, **8**, 6922–6933.
38 L. Cheng, K. Yang, Y. Li, J. Chen, C. Wang, M. Shao, S.-T. Lee and Z. Liu, *Angew. Chem., Int. Ed.*, 2011, **50**, 7385–7390.
39 R. Lv, D. Yang, P. Yang, J. Xu, F. He, S. Gai, C. Li, Y. Dai, G. Yang and J. Lin, *Chem. Mater.*, 2016, **28**, 4724–4734.
40 M. Chen, X. Fang, S. Tang and N. Zheng, *Chem. Commun.*, 2012, **48**, 8934–8936.
41 L. Cheng, K. Yang, Q. Chen and Z. Liu, *ACS Nano*, 2012, **6**, 5605–5613.
42 Y. Liu, K. Ai, J. Liu, M. Deng, Y. He and L. Lu, *Adv. Mater.*, 2013, **25**, 1353–1359.
43 E. I. Yslas, L. E. Ibarra, M. A. Molina, C. Rivarola, C. A. Barbero, M. L. Bertuzzi and V. A. Rivarola, *J. Nanopart. Res.*, 2015, **17**, 389.
44 L. E. Ibarra, E. I. Yslas, M. A. Molina, C. Rivarola, S. Romanini, C. A. Barbero, V. A. Rivarola and M. L. Bertuzzi, *Laser Phys.*, 2013, **23**, 1–7.
45 Y. Zhao, T. Ji, H. Wang, S. Li, Y. Zhao and G. Nie, *J. Controlled Release*, 2014, **177**, 11–19.
46 L. Wang and C. Li, *J. Mater. Chem.*, 2011, **21**, 15862–15871.
47 C. H. Tung, J. Qi, L. Hu, M. S. Han and Y. Kim, *Theranostics*, 2015, **5**, 1166–1174.
48 L. Dong, S. Xia, K. Wu, Z. Huang, H. Chen, J. Chen and J. Zhang, *Biomaterials*, 2010, **31**, 6309–6316.
49 A. Zhu, K. Miao, Y. Deng, H. Ke, H. He, T. Yang, M. Guo, Y. Li, Z. Guo, Y. Wang, X. Yang, Y. Zhao and H. Chen, *ACS Nano*, 2015, **9**, 7874–7885.
50 L. Li, J. Gu, J. Zhang, Z. Xie, Y. Lu, L. Shen, Q. Dong and Y. Wang, *ACS Appl. Mater. Interfaces*, 2015, **7**, 8033–8040.

 This journal is © The Royal Society of Chemistry 2017